Gamma-ray bursts: afterglows from cylindrical jets

K. S. Cheng,[1] $\star$ Y. F. Huang[2,3,4] $\star$ and T. Lu[2,4] $\star$

[1]*Department of Physics, The University of Hong Kong, Pokfulam Road, Hong Kong, China*

[2]*Department of Astronomy, Nanjing University, Nanjing 210093, China*

[3]*Astronomical and Astrophysical Center of East China, Nanjing University, Nanjing 210093, China*

[4]*LCRHEA, Institute for High-Energy Physics, Chinese Academy of Sciences, Beijing 100039, China*

ABSTRACT

Nearly all previous discussion on beaming effects in gamma-ray bursts have assumed a conical geometry. However, more and more observations on relativistic jets in radio galaxies, active galactic nuclei, and "microquasars" in the Galaxy have shown that many of these outflows are not conical, but cylindrical, i.e., they maintain constant cross sections at large scales. Thus it is necessary to discuss the possibility that gamma-ray bursts may be due to highly collimated cylindrical jets, not conical ones. Here we study the dynamical evolution of cylindrical jets and discuss their afterglows. Both analytical and numerical results are presented. It is shown that when the lateral expansion is not taken into account, a cylindrical jet typically remains to be highly relativistic for $\sim 10^8$ — 10^9 s. During this relativistic phase, the optical afterglow decays as $S_\nu \propto t^{-p/2}$ at first, where p is the index characterizing the power-law energy distribution of electrons. Then the light curve steepens to be $S_\nu \propto t^{-(p+1)/2}$ due to cooling of electrons. After entering the non-relativistic phase (i.e., $t \geq 10^{11}$ s), the afterglow is $S_\nu \propto t^{-(5p-4)/6}$. But if the cylindrical jet expands laterally at co-moving sound speed, then the decay becomes $S_\nu \propto t^{-p}$ and $S_\nu \propto t^{-(15p-21)/10}$ — $t^{-(15p-20)/10}$ in the ultra-relativistic and non-relativistic phase respectively. Note that in both cases, the light curve turns flatter after the relativistic-Newtonian transition point, which differs markedly from the behaviour of a conical jet. It is suggested that some gamma-ray bursts with afterglows decaying as $t^{-1.1}$ — $t^{-1.3}$ may be due to cylindrical jets, not necessarily isotropic fireballs.

1 INTRODUCTION

The discovery of gamma-ray burst (GRB) afterglows in early 1997 (van Paradijs et al. 1997; Sahu et al. 1997) has revolutionized the researches in the field (Wijers 1998). Since then, X-ray afterglows (Costa et al. 1997; Piro et al. 1998) have been detected from more than 20 GRBs, of which a half were observed optically (e.g., Groot et al. 1997; Galama et al. 1997; Metzger et al. 1997; Kulkarni et al. 1998; Pedersen et al. 1998; Garcia et al. 1998; Akerlof et al. 1999; Vreeswijk et al. 1999) and one third were even observed in radio bands (e.g., Frail et al. 1997; Galama et al. 1998a, b). The cosmological origin is thus firmly established, and the so called fireball model (Goodman 1986; Paczyński 1986; Rees & Mészáros 1992, 1994; Mészáros & Rees 1992; Mészáros, Laguna & Rees 1993; Mészáros, Rees & Papathanassiou 1994; Katz 1994; Sari, Narayan & Piran 1996) becomes the most popular model, which is found successful in explaining the global features of GRB afterglows (Mészáros & Rees 1997; Waxman 1997a, b; Tavani 1997; Vietri 1997; Wijers, Rees & Mészáros 1997; Mészáros, Rees & Wijers 1998; Sari, Piran & Narayan 1998; Dermer et al. 1999a, b; Wijers & Galama 1999; Dai & Lu 1998, 1999). For detailed reviews on recent progresses, see Piran (1999) and van Paradijs, Kouveliotou & Wijers (2000).

However, we are still far from resolving the puzzle of GRBs, because many crucial problems are largely open. For example, whether a GRB is due to a highly collimated jet or an isotropic fireball is still controversial. This issue has been discussed extensively. It is generally believed that due to both the edge effect (Panaitescu & Mészáros 1999; Kulkarni et al. 1999; Mészáros & Rees 1999) and the lateral expansion effect (Rhoads 1997, 1999), afterglows from a jet will be characterized by a break in the light curve during the relativistic phase. GRBs 990123, 990510 and 000301c are regarded as good examples (Kulkarni et al. 1999; Harrison et al. 1999; Castro-Tirado et al. 1999; Sari, Piran & Halpern 1999; Wijers et al. 1999; Rhoads & Fruchter 2001; Berger et al. 2001; Jensen et al. 2001; Masetti et al. 2000). But detailed numerical studies show that the break is usually quite smooth (Panaitescu & Mészáros 1998; Moderski, Sikora & Bulik 2000). Recently Huang et al. (1998a, b, 1999a,

⋆ E-mail: hrspksc@hkucc.hku.hk(KSC); hyf@nju.edu.cn(YFH); tlu@nju.edu.cn(TL)

b) stressed the importance of the non-relativistic phase of GRB afterglows. They have used their refined dynamical model to discuss afterglows from jetted GRB remnants (Huang et al. 2000a, b, c). It is found that the most obvious light curve break does not appear in the relativistic phase, but occurs at the relativistic-Newtonian transition point. They also stressed that the break is parameter-dependent (Huang et al. 2000b). Based on their investigations, the rapid fading of optical afterglows from GRBs 970228, 980326, 980519, 990123, 990510 and 991208 has been suggested as evidence for beaming in these cases (Huang et al. 2000d).

In all these discussion, a conical jet (i.e., a jet with a constant half opening angle; of course, in some more realistic discussion, the conical jet is permitted to expand laterally) has been assumed. However, we should note that this might not be the case. For example, we know that a relativistic flow (i.e., a jet) is a common feature of radio galaxies. Interestingly, copious examples have shown that these outflows are not conical, instead, they maintain constant cross sections at large scales (Perley, Bridle & Willis 1984; Biretta, Sparks & Macchetto 1999; also see GLAST home page: *http://www-glast.sonoma.edu/gru/agn/Default.htm* and Chandra home page: *http://chandra.harvard.edu/photo/cycle1/pictor/index.html* for good examples). Here we call a jet maintaining a constant cross section a cylindrical jet. It is reasonable to deduce that ultra-relativistic outflows in GRBs might also be cylindrical jets, not conical ones. In fact, this idea has already been suggested as GRB trigger mechanism by Dar et al. (Shaviv & Dar 1995; Dar 1998, 1999).

Afterglows from a cylindrical jet is likely to differ from those of a conical jet markedly. If GRBs are really due to cylindrical jets, then we need to examine their dynamics and afterglows in detail, which is just the purpose of this article. The structure of our article is as follows. We describe our model in Section 2 and present the analytic solution in Section 3. Section 4 is the numerical results and Section 5 is brief discussion.

2 MODEL

Let us consider a highly collimated GRB remnant, ploughing its way through a homogeneous interstellar medium (ISM) where the number density is n. Denote the lateral radius of the remnant as a, and its distance from the central engine of the GRB as R. The remnant will maintain a constant cross section (i.e., $a \equiv$ const), except that it may expand laterally at a speed $v_\perp$.

4

2.1 Dynamics

In the literature, the following differential equation is usually used to depict the expansion of GRB remnants (e.g., Chiang & Dermer 1999; Piran 1999),

$$\frac{d\gamma}{dm} = -\frac{\gamma^2 - 1}{M}, \tag{1}$$

where m is the rest mass of the swept-up medium, γ is the bulk Lorentz factor and M is the total mass in the co-moving frame, including internal energy. However, Huang et al. (1999a, b) pointed out that in the adiabatic case equation (1) does not match with the Sedov solution during the non-relativistic phase. They have proposed a refined equation,

$$\frac{d\gamma}{dm} = -\frac{\gamma^2 - 1}{M_{\rm ej} + \epsilon m + 2(1 - \epsilon)\gamma m}, \tag{2}$$

which is shown to be correct for both adiabatic and highly radiative shocks, and in both relativistic and Newtonian phase. Here $M_{\rm ej}$ is the initial ejecta mass and ϵ is the radiative efficiency. In this paper we adopt equation (2) to describe the dynamical behavior of our cylindrical jet. For simplicity, we will only consider the adiabatic case (i.e., $\epsilon \equiv 0$).

The evolution of radius (R), the swept-up mass (m), and the lateral radius (a) is described by (cf. Huang et al. 2000a, b),

$$\frac{dR}{dt} = \beta c\gamma(\gamma + \sqrt{\gamma^2 - 1}), \tag{3}$$

$$\frac{dm}{dR} = \pi a^2 n m_{\rm p}, \tag{4}$$

$$\frac{da}{dt} = v_\perp(\gamma + \sqrt{\gamma^2 - 1}), \tag{5}$$

where t is the observer's time, $\beta = \sqrt{\gamma^2 - 1}/\gamma$, c is the speed of light, and $m_{\rm p}$ is the mass of proton. As for $v_\perp$, we have two possibilities, just like in the case of a conical jet: (i) $v_\perp \equiv 0$, this means the jet does not expand laterally, it maintains a constant cross section strictly. The problem is then greatly simplified; (ii) $v_\perp \equiv c_{\rm s}$, i.e., the jet expands laterally at the co-moving sound speed, of which a reasonable expression has been derived by Huang et al. (2000a, b) as,

$$c_{\rm s}^2 = \hat{\gamma}(\hat{\gamma} - 1)(\gamma - 1)\frac{1}{1 + \hat{\gamma}(\gamma - 1)}c^2, \tag{6}$$

where $\hat{\gamma} \approx (4\gamma + 1)/(3\gamma)$ is the adiabatic index (Dai, Huang & Lu 1999). In the ultra-relativistic limit ($\gamma \gg 1, \hat{\gamma} \approx 4/3$), equation (6) gives $c_{\rm s}^2 = c^2/3$; and in the non-relativistic limit ($\gamma \sim 1, \hat{\gamma} \approx 5/3$), we simply get $c_{\rm s}^2 = 5\beta^2 c^2/9$.

Equations (2) — (5) give a thorough description of the dynamical evolution of our cylindrical jets. We will solve them analytically in the next section and then present our numerical results in Section 4.

2.2 Synchrotron radiation

A strong blastwave will be produced due to the interaction of the remnant with the ISM. Synchrotron radiation from the shock-accelerated ISM electrons gives birth to GRB afterglows. As usual, we assume that the magnetic energy density in the co-moving frame is a fraction ξ_B^2 of the total thermal energy density ($B'^2/8\pi = \xi_B^2 e'$), and that electrons carry a fraction ξ_e of the proton energy, which means that the minimum Lorentz factor of the random motion of electrons in the co-moving frame is $\gamma_{e,\min} = \xi_e(\gamma - 1)m_p/m_e + 1$, where m_e is the electron mass. In the absence of radiation loss, the distribution of the shock-accelerated electrons behind the blastwave can be characterized by a power-law function of electron energy, $dN'_e/d\gamma_e \propto \gamma_e^{-p}$ ($\gamma_{e,\min} \leq \gamma_e \leq \gamma_{e,\max}$), where $\gamma_{e,\max}$ is the maximum Lorentz factor, $\gamma_{e,\max} = 10^8 (B'/1\mathrm{G})^{-1/2}$ (Mészáros et al. 1993; Vietri 1997; Dai et al. 1999).

However, radiation loss may play an important role in the process. Sari et al. (1998) have derived an equation for the critical electron Lorentz factor, γ_c, above which synchrotron radiation is significant:

$$\gamma_c = 6\pi m_e c/(\sigma_T \gamma B'^2 t), \tag{7}$$

where σ_T is the Thompson cross section. The distribution of radiative electrons (i.e., those with $\gamma_e > \gamma_c$) becomes another power-law function of $dN'_e/d\gamma_e \propto \gamma_e^{-(p+1)}$. A good description of electron distribution allowing for radiation loss has been presented by Dai et al. (1999, also see: Huang et al. 2000a, b). We will use their expression in this research. For convenience, let us define a characteristic frequency of $\nu_c \equiv \gamma \gamma_c^2 e B'/(2\pi m_e c)$ here (Sari et al. 1998).

In the co-moving frame, synchrotron radiation power at frequency ν' from electrons is given by (Rybicki & Lightman 1979),

$$P'(\nu') = \frac{\sqrt{3}e^3 B'}{m_e c^2} \int_{\gamma_{e,\min}}^{\gamma_{e,\max}} \left(\frac{dN'_e}{d\gamma_e}\right) F\left(\frac{\nu'}{\nu'_{cr}}\right) d\gamma_e, \tag{8}$$

where e is electron charge, $\nu'_{cr} = 3\gamma_e^2 e B'/(4\pi m_e c)$, and

$$F(x) = x \int_x^{+\infty} K_{5/3}(k)dk, \tag{9}$$

with $K_{5/3}(k)$ being the Bessel function. We assume that this power is radiated isotropically,

$$\frac{dP'(\nu')}{d\Omega'} = \frac{P'(\nu')}{4\pi}. \tag{10}$$

Let Θ be the angle between the axis of the jet and the line of sight, and define $\mu = \cos\Theta$, we can derive the angular distribution of power in the observer's frame (Rybicki & Lightman 1979),

$$\frac{dP(\nu)}{d\Omega} = \frac{1}{\gamma^3(1-\beta\mu)^3}\frac{dP'(\nu')}{d\Omega'} = \frac{1}{\gamma^3(1-\beta\mu)^3}\frac{P'(\nu')}{4\pi}, \tag{11}$$

$$\nu = \frac{\nu'}{\gamma(1-\mu\beta)}. \tag{12}$$

Then the observed flux density at frequency ν is (Huang et al. 2000a, b),

$$S_\nu = \frac{1}{A}\left(\frac{dP(\nu)}{d\Omega}\frac{A}{D_\mathrm{L}^2}\right) = \frac{1}{\gamma^3(1-\beta\mu)^3}\frac{1}{4\pi D_\mathrm{L}^2}P'\left(\gamma(1-\mu\beta)\nu\right), \tag{13}$$

where A is the area of our detector and D_L is the luminosity distance.

3 ANALYTIC SOLUTIONS

Since the geometry concerned here is still quite simple, we can derive approximate solutions to the problem analytically. In this section, for simplicity, we assume $\Theta = 0$, i.e., the jet is just moving along the line of sight. Obviously, we then do not need to consider the effect of the equal arrival time surfaces (Waxman 1997b; Sari 1997; Panaitescu & Mészáros 1998). We discuss the two cases of $v_\perp \equiv 0$ and $v_\perp \equiv c_\mathrm{s}$ separately. Note that we take $\epsilon \equiv 0$ all through the article.

3.1 $v_\perp \equiv 0$ case

During the ultra-relativistic phase, since $\gamma \gg 1$, $\beta \approx 1$, and $\gamma m \gg M_\mathrm{ej}$, equations (2) — (5) reduce to,

$$\frac{d\gamma}{dm} \approx -\frac{\gamma}{2m}, \quad \frac{dm}{dR} \approx \mathrm{const}, \quad \frac{dR}{dt} \approx 2\gamma^2 c. \tag{14}$$

Then it is very easy to get:

$$\gamma \propto m^{-1/2}, \quad m \propto R, \quad R \propto t^{1/2}. \tag{15}$$

Additionally, from the shock conditions (Blandford & McKee 1976; Huang et al. 1998a, b), the co-moving thermal energy density is $e' \propto \gamma^2 \propto t^{-1/2}$, so we have $B' \propto (e')^{1/2} \propto t^{-1/4}$, and $\nu_\mathrm{c} \propto \gamma\gamma_\mathrm{c}^2 B' \propto t^{-1}$. Since the peak frequency of synchrotron radiation is $\nu_\mathrm{m} \propto \gamma\gamma_\mathrm{e,min}^2 B'$ (Sari et al. 1998), we have $\nu_\mathrm{m} \propto t^{-1}$, and the peak flux density is $S_{\nu,\mathrm{max}} \propto N_\mathrm{e}\gamma B'/\gamma^{-2} \propto$

$N_e \gamma^3 B' \propto t^{-1/2}$. The factor of γ^{-2} in $S_{\nu,\mathrm{max}}$ is due to the relativistic beaming effect. At last, we can derive the flux density of the afterglow as follows,

$$
S_\nu \approx
\begin{cases}
S_{\nu,\mathrm{max}} \left(\frac{\nu}{\nu_\mathrm{m}}\right)^{-(p-1)/2} \propto \nu^{-(p-1)/2} t^{-p/2}, & (\nu_\mathrm{m} \leq \nu < \nu_\mathrm{c}, \text{ slow cooling}), \\[2ex]
S_{\nu,\mathrm{max}} \left(\frac{\nu_\mathrm{c}}{\nu_\mathrm{m}}\right)^{-(p-1)/2} \left(\frac{\nu}{\nu_\mathrm{c}}\right)^{-p/2} \propto \nu^{-p/2} t^{-(p+1)/2}, & (\nu_\mathrm{m} < \nu_\mathrm{c} \leq \nu, \text{ slow cooling}), \\[2ex]
S_{\nu,\mathrm{max}} \left(\frac{\nu}{\nu_\mathrm{c}}\right)^{-1/2} \propto \nu^{-1/2} t^{-1}, & (\nu_\mathrm{c} \leq \nu < \nu_\mathrm{m}, \text{ fast cooling}), \\[2ex]
S_{\nu,\mathrm{max}} \left(\frac{\nu_\mathrm{m}}{\nu_\mathrm{c}}\right)^{-1/2} \left(\frac{\nu}{\nu_\mathrm{m}}\right)^{-p/2} \propto \nu^{-p/2} t^{-(p+1)/2}, & (\nu_\mathrm{c} < \nu_\mathrm{m} \leq \nu, \text{ fast cooling}).
\end{cases}
\tag{16}
$$

In the non-relativistic phase, $\gamma \sim 1$, $\beta \ll 1$, $d\gamma \approx \beta d\beta$, equations (2) — (5) reduce to,

$$
\frac{d\beta}{dm} \approx -\frac{\beta}{2m}, \quad \frac{dm}{dR} \approx \text{const}, \quad \frac{dR}{dt} \approx \beta c.
\tag{17}
$$

The scaling laws become,

$$
\beta \propto m^{-1/2}, \quad m \propto R, \quad R \propto t^{2/3}.
\tag{18}
$$

According to the shock conditions (Huang et al. 1998a, b), the co-moving thermal energy density is $e' \propto \gamma - 1 \propto t^{-2/3}$. Then we have $B' \propto (e')^{1/2} \propto t^{-1/3}$, $\nu_\mathrm{c} \propto \gamma \gamma_\mathrm{c}^2 B' \propto t^{-1}$, $\nu_\mathrm{m} \propto \gamma \gamma_{\mathrm{e,min}}^2 B' \propto t^{-5/3}$, $S_{\nu,\mathrm{max}} \propto \gamma N_e B' \propto t^{1/3}$, and finally the flux density is,

$$
S_\nu \approx
\begin{cases}
S_{\nu,\mathrm{max}} \left(\frac{\nu}{\nu_\mathrm{m}}\right)^{-(p-1)/2} \propto \nu^{-(p-1)/2} t^{-(5p-7)/6}, & (\nu_\mathrm{m} \leq \nu < \nu_\mathrm{c}, \text{ slow cooling}), \\[2ex]
S_{\nu,\mathrm{max}} \left(\frac{\nu_\mathrm{c}}{\nu_\mathrm{m}}\right)^{-(p-1)/2} \left(\frac{\nu}{\nu_\mathrm{c}}\right)^{-p/2} \propto \nu^{-p/2} t^{-(5p-4)/6}, & (\nu_\mathrm{m} < \nu_\mathrm{c} \leq \nu, \text{ slow cooling}), \\[2ex]
S_{\nu,\mathrm{max}} \left(\frac{\nu}{\nu_\mathrm{c}}\right)^{-1/2} \propto \nu^{-1/2} t^{-1/6}, & (\nu_\mathrm{c} \leq \nu < \nu_\mathrm{m}, \text{ fast cooling}), \\[2ex]
S_{\nu,\mathrm{max}} \left(\frac{\nu_\mathrm{m}}{\nu_\mathrm{c}}\right)^{-1/2} \left(\frac{\nu}{\nu_\mathrm{m}}\right)^{-p/2} \propto \nu^{-p/2} t^{-(5p-4)/6}, & (\nu_\mathrm{c} < \nu_\mathrm{m} \leq \nu, \text{ fast cooling}).
\end{cases}
\tag{19}
$$

Let us discuss the decay of optical afterglows (e.g., R band, at the frequency ν_R) in more detail. In the ultra-relativistic phase, $\nu_\mathrm{m} \ll \nu_\mathrm{R} \ll \nu_\mathrm{c}$ is typically satisfied initially, then we have $S_\mathrm{R} \propto \nu^{-(p-1)/2} t^{-p/2}$ at early stages. Since ν_m and ν_c both scale as t^{-1}, we will eventually have $\nu_\mathrm{m} < \nu_\mathrm{c} < \nu_\mathrm{R}$, then the afterglow at later stages is just $S_\mathrm{R} \propto \nu^{-p/2} t^{-(p+1)/2}$, i.e., the light curve steepens by $t^{1/2}$ due to the cooling effect of electrons. After entering the non-relativistic phase, since $\nu_\mathrm{m} \propto t^{-5/3}$ and $\nu_\mathrm{c} \propto t^{-1}$, the relation of $\nu_\mathrm{m} < \nu_\mathrm{c} < \nu_\mathrm{R}$ will continue to be satisfied. The afterglow then decays as $S_\mathrm{R} \propto \nu^{-p/2} t^{-(5p-4)/6}$, which means the light curve usually becomes flatter again, by $t^{(7-2p)/6}$

3.2 $v_\perp \equiv c_{\rm s}$ case

During the ultra-relativistic phase, $\gamma \gg 1$, $\beta \approx 1$, $\gamma m \gg M_{\rm ej}$, $c_{\rm s} \approx c/\sqrt{3}$, equations (2) — (5) reduce to,

$$\frac{d\gamma}{dm} \approx -\frac{\gamma}{2m}, \quad \frac{dm}{dR} \approx \pi a^2 n m_{\rm p}, \quad \frac{da}{dt} \approx \frac{2\gamma c}{\sqrt{3}}, \quad \frac{dR}{dt} \approx 2\gamma^2 c. \tag{20}$$

The corresponding solution is,

$$\gamma \propto t^{-1/2}, \quad a \propto t^{1/2}, \quad m \propto t. \tag{21}$$

Similarly we have $e' \propto \gamma^2 \propto t^{-1}$, $B' \propto (e')^{1/2} \propto t^{-1/2}$, $\nu_{\rm c} \propto \gamma\gamma_{\rm c}^2 B' \propto t^0$, $\nu_{\rm m} \propto \gamma\gamma_{\rm e,min}^2 B' \propto t^{-2}$, and $S_{\nu,\rm max} \propto N_{\rm e}\gamma B'/\gamma^{-2} \propto t^{-1}$. The flux density of the afterglow is then given by,

$$S_\nu \approx \begin{cases} S_{\nu,\rm max}\left(\frac{\nu}{\nu_{\rm m}}\right)^{-(p-1)/2} \propto \nu^{-(p-1)/2}t^{-p}, & (\nu_{\rm m} \leq \nu < \nu_{\rm c}, \text{ slow cooling}), \\[3ex] S_{\nu,\rm max}\left(\frac{\nu_{\rm c}}{\nu_{\rm m}}\right)^{-(p-1)/2}\left(\frac{\nu}{\nu_{\rm c}}\right)^{-p/2} \propto \nu^{-p/2}t^{-p}, & (\nu_{\rm m} < \nu_{\rm c} \leq \nu, \text{ slow cooling}), \\[3ex] S_{\nu,\rm max}\left(\frac{\nu}{\nu_{\rm c}}\right)^{-1/2} \propto \nu^{-1/2}t^{-1}, & (\nu_{\rm c} \leq \nu < \nu_{\rm m}, \text{ fast cooling}) \\[3ex] S_{\nu,\rm max}\left(\frac{\nu_{\rm m}}{\nu_{\rm c}}\right)^{-1/2}\left(\frac{\nu}{\nu_{\rm m}}\right)^{-p/2} \propto \nu^{-p/2}t^{-p}, & (\nu_{\rm c} < \nu_{\rm m} \leq \nu, \text{ fast cooling}). \end{cases} \tag{22}$$

Note that in most cases, the flux density decays as t^{-p}.

In the non-relativistic phase, $\gamma \sim 1$, $\beta \ll 1$, $c_{\rm s} \approx \sqrt{5}\beta c/3$, equations (2) — (5) reduce to,

$$\frac{d\beta}{dm} \approx -\frac{\beta}{2m}, \quad \frac{dm}{dR} \approx \pi a^2 n m_{\rm p}, \quad \frac{da}{dt} \approx \frac{\sqrt{5}\beta c}{3}, \quad \frac{dR}{dt} \approx \beta c. \tag{23}$$

The solution is also easy to get as,

$$\beta \propto m^{-1/2}, \quad m \propto R^3, \quad R \propto a \propto t^{2/5}. \tag{24}$$

Then we have: $e' \propto \gamma - 1 \propto t^{-6/5}$, $B' \propto (e')^{1/2} \propto t^{-3/5}$, $\nu_{\rm c} \propto \gamma\gamma_{\rm c}^2 B' \propto t^{-1/5}$, $\nu_{\rm m} \propto \gamma\gamma_{\rm e,min}^2 B' \propto \beta^4 B' \propto t^{-3}$, $S_{\nu,\rm max} \propto \gamma N_{\rm e} B' \propto t^{3/5}$. So the flux density is,

$$S_\nu \approx \begin{cases} S_{\nu,\rm max}\left(\frac{\nu}{\nu_{\rm m}}\right)^{-(p-1)/2} \propto \nu^{-(p-1)/2}t^{-(15p-21)/10}, & (\nu_{\rm m} \leq \nu < \nu_{\rm c}, \text{ slow cooling}), \\[3ex] S_{\nu,\rm max}\left(\frac{\nu_{\rm c}}{\nu_{\rm m}}\right)^{-(p-1)/2}\left(\frac{\nu}{\nu_{\rm c}}\right)^{-p/2} \propto \nu^{-p/2}t^{-(15p-20)/10}, & (\nu_{\rm m} < \nu_{\rm c} \leq \nu, \text{ slow cooling}), \\[3ex] S_{\nu,\rm max}\left(\frac{\nu}{\nu_{\rm c}}\right)^{-1/2} \propto \nu^{-1/2}t^{1/2}, & (\nu_{\rm c} \leq \nu < \nu_{\rm m}, \text{ fast cooling}), \\[3ex] S_{\nu,\rm max}\left(\frac{\nu_{\rm m}}{\nu_{\rm c}}\right)^{-1/2}\left(\frac{\nu}{\nu_{\rm m}}\right)^{-p/2} \propto \nu^{-p/2}t^{-(15p-20)/10}, & (\nu_{\rm c} < \nu_{\rm m} \leq \nu, \text{ fast cooling}). \end{cases} \tag{25}$$

Again let us have a look at the R band optical light curve. In the ultra-relativistic phase, typically we have $\nu_m \ll \nu_R \ll \nu_c$, so the afterglow decays as $S_R \propto \nu^{-(p-1)/2}t^{-p}$. After entering the non-relativistic phase, we will have $\nu_m \leq \nu_R < \nu_c$ at first, which means $S_R \propto \nu^{-(p-1)/2}t^{-(15p-21)/10}$. We see that the light curve becomes flatter by $t^{(21-5p)/10}$. Since ν_c now decreases as $\nu_c \propto t^{-1/5}$, at sufficiently late stages, we will eventually have $\nu_m < \nu_c < \nu_R$, which leads to $S_R \propto \nu^{-p/2}t^{-(15p-20)/10}$, i.e., the light curve is still flatter than that in the relativistic phase (by $t^{(20-5p)/10}$). In short, after entering the non-relativistic phase, the light curve is expected to become flatter obviously, which is quite different from the behaviour of a laterally expanding conical jet (Huang et al. 2000a, b, c, d).

4 NUMERICAL RESULTS

Now we solve equations (2) — (5) numerically and compare the optical (R band) afterglow light curves with those of conical jets. First we describe our initial values and parameters briefly. The ISM density (n), the original ejecta mass (M_{ej}) and the initial value of γ are fixedly set as $n = 1$ cm^{-3}, $M_{ej} = 5 \times 10^{-10}M_\odot$, and $\gamma_0 = 300$, respectively. We further assume $a_0 = 1.2 \times 10^{14}$ cm, then the initial values of m and R are given by: $m_0 = M_{ej}/300$, $R_0 = m_0/(\pi a_0^2 n m_p) \approx 1.2 \times 10^{17}$ cm. These values indicate that the angular radius of our GRB ejecta from the central engine is only $\sim 10^{-3}$ at the beginning, and in the ultra-relativistic phase considered here it is just as powerful as an isotropic fireball with kinetic energy $E_{iso,0} \sim 10^{54}$ ergs. In calculating the R band flux densities, we take $D_L = 1$ Gpc, and will assume $p = 2.5$, $\xi_e = 0.1$, $\xi_B^2 = 10^{-6}$, $\Theta = 0$ unless declared explicitly.

Here, we would like to point out that many of our initial values and parameters (such as n, M_{ej}, γ_0, a_0 and D_L) have been arbitrarily chosen. However, variation of them within reasonable ranges will not alter the major conclusions we draw below in this section.

4.1 $v_\perp \equiv 0$ case

Assuming no lateral expansion, we have evaluated equations (2) — (5) numerically. Fig. 1 shows the evolution of the Lorentz factor, γ. The jet becomes non-relativistic after $\sim 10^{11}$ s. In the relativistic phase the slope is approximately -0.26 and in the non-relativistic phase it is about -0.68, both consistent with the theoretical value (i.e., $-1/4$ and $-2/3$ respectively, see Section 3.1). For comparison, the dashed line shows the evolution of γ for a conical jet

(parameters: $E_{\mathrm{iso},0} = 10^{54}$ ergs, $\gamma_0 = 300$, with an initial half opening angle $\theta_0 = 0.1$). We see that the cylindrical jet decelerates much slower, which is easy to understand.

Fig. 2 illustrates the Lorentz factor as a function of R. The slope of the solid line is -1.00 in the relativistic phase and -0.50 in the non-relativistic phase, also consistent with the theoretical results. This further confirms the correctness of our programs.

The R band afterglow light curves are shown in Fig. 3. The solid line represents a cylindrical jet with $p = 2.5$. Its slope is approximately -1.26 before 10^9 s, consistent with the theoretical value of -1.25 (for $\nu_{\mathrm{m}} < \nu_{\mathrm{R}} < \nu_{\mathrm{c}}$ case, see Section 3.1). The slope is -1.89 between 10^{10} s and 10^{11} s, also in good agreement with our analytical results (-1.75 for $\nu_{\mathrm{m}} < \nu_{\mathrm{c}} < \nu_{\mathrm{R}}$). After $\sim 10^{11}$ s, the jet enters the non-relativistic phase and the light curve becomes flatter slightly, just as required by the theoretical result. The dotted line here represents afterglows from a conical jet ($p = 2.5$). We can see that the light curve of a cylindrical jet differs markedly from that of a conical one, mainly in the following two aspects: (i) the relativistic phase lasts for a very long period ($> 10^{10}$ s typically), during which only a slight break (by $t^{1/2}$, due to cooling of electrons) can be observed; (ii) after entering the Newtonian phase, it becomes flatter slightly, not steeper. Please note that at the end point of each line, the characteristic Lorentz factor of electrons has already been as small as $\gamma_{\mathrm{e}} \sim 5$.

Fig. 4 illustrates the effect of three parameters, ξ_{e}, ξ_{B}^2 and Θ, on the light curve. It is clear that ξ_{e} does not change the shape of the light curve markedly. However, because ν_{c} strongly depends on B' ($\gamma_{\mathrm{c}} \propto B'^{-2}$, $\nu_{\mathrm{c}} \propto B'^{-3}$), we see that ξ_{B}^2 affects the cooling break seriously. In our calculations, since we take $\gamma_0 = 300$, we have found that for any Θ smaller than $1/300$, the light curve will be almost identical to the $\Theta = 0$ case. But in the $\Theta = 0.1$ case, the flux density is lowered down markedly before $\sim 10^7$ s, which means a cylindrical jet is observable only within a narrow solid angle.

4.2 $v_\perp \equiv c_{\mathrm{s}}$ case

When lateral expansion is included, the results are quite different. The solid line in Fig. 5 illustrates the evolution of γ in this case. We can see that the jet becomes Newtonian at $\sim 10^5$ — 10^6 s, much earlier than the $v_\perp \equiv 0$ case. Note that its slope is approximately -0.51 in the ultra-relativistic phase and -1.20 in the non-relativistic phase, both consistent with the theoretical values (i.e., $-1/2$ and $-6/5$ respectively, see Section 3.2). Fig. 5 also

shows that when $v_\perp \equiv c_s$, a cylindrical jet decelerates faster than a conical one, which is just contrary to the $v_\perp \equiv 0$ case. The $\gamma - R$ relation is shown in Fig. 6 by the solid line. In the non-relativistic phase, the slope is ~ -3.0, consistent with the theoretical value. However, in the ultra-relativistic phase, the $\gamma - R$ relation is not a power-law function, but an exponential one.

Fig. 7 illustrates the evolution of the jet profile on the $y - z$ plane. Generally speaking, the lateral expansion is not significant during the ultra-relativistic phase. But in the non-relativistic phase, the lateral radius increases synchronically with the radial scale.

R band afterglows from cylindrical jets expanding laterally are shown in Fig. 8. The solid line is plot with $p = 2.5$. Its slope is ~ -2.63 before 10^6 s, consistent with the theoretical value of -2.5 (see Section 3.2). It turns flatter in the non-relativistic phase, also consistent with our analytical results. The dotted line corresponds to a laterally expanding conical jet ($p = 2.5$), where a break due to the relativistic-Newtonian transition can be clearly seen (Huang et al. 2000a, b, c, d). It is clear that the light curve of a cylindrical jet differs from that of a conical one mainly in the following aspects: (i) no obvious breaks could be observed; (ii) in the relativistic phase, the decay is always as quick as t^{-p}, but for a conical jet the decay is only $t^{-(3p-3)/4}$ at early stages (Rhoads 1997, 1999); (iii) after entering the non-relativistic phase, the light curve becomes flatter slightly, also quite different from that of a conical jet. Fig. 9 illustrates the effect of ξ_e, ξ_B^2 and Θ on the light curve. Similar to the $v_\perp \equiv 0$ case, the flux density is markedly lowered down by a non-zero Θ, but generally speaking, ξ_e and ξ_B^2 do not change the slope of the light curve here.

5 DISCUSSION AND CONCLUSIONS

The importance of collimation in GRBs goes beyond influencing the detailed shape of the light curve: it reveals something about the central engine, and affects our estimates of how many GRB progenitors there need to be (van Paradijs et al. 2000; Wijers et al. 1998; Lee, Brown & Wijers 2000). Most theorists now expect GRBs to be significantly collimated, because jets seem to be produced by all systems where matter is undergoing disk accretion onto a compact central object, including young protostars, "microquasars" (i.e., black hole binaries in the Galaxy), capture of a main sequence star by a moderate massive black hole in normal galaxies (Cheng & Lu 2000), radio galaxies, and active galactic nuclei (Lamb 2001). Observations on these systems have interestingly indicated that an astrophysical jet usually

maintains a constant cross section at large scales (Perley et al. 1984; Biretta et al. 1999). In fact, it has already been pointed out by Dar et al. (Shaviv & Dar 1995; Dar 1998, 1999) that although a conical beam can solve the "energy crisis" of GRBs, it suffers from some other deficiencies of isotropic fireballs, while a cylindrical jet does not. However, nearly all previous discussion on afterglows from collimated GRB remnants have assumed a conical geometry, which, we believe is not enough. Here we have discussed afterglows from cylindrical jets in detail. Both analytic and numerical results are presented.

For a cylindrical jet without lateral expansion, in the relativistic phase the flux density typically decays as $S_\nu \propto t^{-p/2}$ at first. Then the light curve steepens by $t^{1/2}$ due to cooling of electrons. After entering the Newtonian phase, the decline becomes slightly slower, $S_\nu \propto t^{-(5p-4)/6}$, just contrary to the behavior of a conical jet. Note that the remnant usually decelerates very slowly in this case, i.e., $\gamma \propto t^{-1/4}$ when $\gamma \gg 1$, so that it keeps to be highly relativistic as long as $t \sim 10^8 - 10^9$ s. When lateral expansion is included and assuming $v_\perp \equiv c_s$, the afterglow light curve is $S_\nu \propto t^{-p}$ in the ultra-relativistic phase, and it flattens to be $S_\nu \propto t^{-(15p-21)/10}$ or $S_\nu \propto t^{-(15p-20)/10}$ in the the non-relativistic phase, also quite different to a conical jet.

In previous sections, we have assumed that the lateral expansion velocity of our cylindrical jet can be either $v_\perp \equiv 0$ or $v_\perp \equiv c_s$ and we have not given a preference for either of these two cases. Now we discuss this question. At the first glance, the $v_\perp \equiv c_s$ seems more realistic. However, observations on relativistic outflows in radio galaxies reveal that lateral expansion is usually unobtrusive (Perley et al. 1984; Biretta et al. 1999). For example, observed profiles are generally quite different from the profile in our Fig. 7. The high degree of collimation and the suppression of lateral expansion is probably due to magnetic confinement (Dar 1998; Mirabel & Rodriguez 1999) and/or the external pressure. We believe that in many cases, even if the cylindrical jet expands laterally, its velocity will be $v_\perp \ll c_s$.

Afterglows from some GRBs, such as GRBs 970508, 971214, 980329 and 980703 have been observed to decay slowly and steadily within a long period (i.e., up to several months, see van Paradijs et al. 2000), with $S_\nu \propto t^{-1.1} - t^{-1.3}$. Although an isotropic fireball is the most natural and popular model for these GRBs, Huang et al. (1998a; also see Dai et al. 1999) pointed out that there is a problem: usually a typical fireball with kinetic energy $E_{\mathrm{iso},0} = 10^{52}$ ergs will become non-relativistic in one or two months, then the theoretical light curve will become steeper slightly (Wijers et al. 1997; Huang et al. 1998b, 1999a, b). So it is difficult to understand why the light curve is a single straight line that lasts for $0.5 - 1$ year

(e.g., GRB 970508). Here we suggest that this kind of GRBs might be due to cylindrical jets (with $v_\perp \ll c_s$): a light curve with slope -1.1 — -1.3 can be easily produced by assuming $2.2 \leq p \leq 2.6$, and the steady decline is explained by the fact that these cylindrical jets are highly relativistic even when $t \sim 10^8$ — 10^9 s. Note that in this model, γ-rays of the initial burst are beamed into a solid angle with the angular radius $\sim 1/\gamma_0$. For $\gamma_0 \sim 300$, the beaming angle is ~ 0.003; and for $\gamma_0 \sim 100$, it is ~ 0.01, which means the energy involved will be greatly reduced.

GRBs 990123, 990510, 991216 and 000301c are characterized by an obvious break in the afterglow light curve. A break steeper than $t^{1/2}$ could not be explained directly by our simple cylindrical jet model, either $v_\perp \equiv 0$ or $v_\perp \equiv c_s$. However, there are many other factors that have not been taken into account in this article, such as the inhomogeneity of ISM (especially $n(R) \propto R^{-2}$, Dai & Lu 1998; Chevalier & Li 2000), and the nature of the lateral expansion. For example, we can imagine that in some cases, since the shock is highly radiative at first (which means the remnant is relatively cool), the magnetic field is much stronger initially, and at the same time the external pressure may be high, then the lateral expansion can be successfully suppressed, which will lead to a flat light curve of $S_\nu \propto t^{-1}$ — $t^{-1.3}$ at early stages. At later stages the lateral expansion takes effect and the light curve becomes $S_\nu \propto t^{-2}$ — t^{-3}. So an obvious break appears. In short, we suggest that the cylindrical jet model should be paid attention to and should be investigated further since it seems to be more realistic than the conical jet model on the observational basis.

Recently, Wang & Loeb (2001) discussed the emission from bow shocks of beamed GRBs. They found that the emitted flux from this bow shock may dominate over the direct emission from the conical jet for lines of sight which are outside the angular radius of the jet emission. The event rate for these lines of sight is thus greatly increased. For typical GRB parameters, they found that the bow shock emission from a jet of half-angle $\sim 5^{\circ}$ is visible out to tens of Mpc in the radio and hundreds of Mpc in the X-rays. In most of our calculations where $\Theta = 0$ is assumed, the bow shock emission generally will not play a dominant role. However, we should bear in mind that the bow shock emission is obviously more important for a cylindrical jet than for a conventional conical jet, since observers of a cylindrical jet are more likely to be situated outside the initial emission cone. For example the bow shock emission may take effect in those $\Theta = 0.1$ cases in Figs. 4 and 9. A direct effect of bow shock emission from cylindrical jets is that the beaming factor will be considerably reduced, so that it will be much easier for us to observe them. We will not go further to calculate

the bow shock emission here. But in the future, if the so called "burstless afterglows" are observed, then the question of bow shock emission will become very important.

Finally we would like to say a few words about the origin of the cylindrical jet. It should not be born a cylinder. In fact, the outflow in a black hole-accreting disk system is likely to be conical *initially*, with the half opening angle $\theta \ll 1$. Assuming $\theta \sim 0.1$, then after propagating to a distance of $R \sim 10^{15}$ cm, it will acquire a lateral radius of $a \sim 10^{14}$ cm. So in our calculation we have implicitly assumed that the jet has become cylindrical before $R \sim 10^{15} - 10^{16}$ cm. We will not go to any further details of the mechanism that makes a conical jet into a cylindrical one here, they are beyond the purpose of this article. However, if our cylindrical jet is really originated from a conical outflow very near to the central black hole, then we can draw an interesting conclusion as follows. Adopting the parameters used in Section 4, our cylindrical jet has a total kinetic energy of $E_{\mathrm{ej}} \equiv \gamma_0 M_{\mathrm{ej}} c^2 \approx 3 \times 10^{47}$ ergs. Since this energy comes from a cone with $\theta \sim 0.1$ when $R \leq 10^{15}$ cm, we can get the corresponding *initial* isotropic energy easily as $E_{\mathrm{iso,ini}} \equiv 4\pi \times E_{\mathrm{ej}}/[2\pi(1 - \cos\theta)] \approx 1.2 \times 10^{50}$ ergs. We have already pointed out in Section 4 that our cylindrical jet looks just as powerful as an isotropic fireball with total kinetic energy $E_{\mathrm{iso,0}} \sim 10^{54}$ ergs at the GRB afterglow stage (i.e., when $R \geq 10^{17}$ cm). So our final conclusion is: if GRBs are really due to cylindrical jets, then an apparently energetic GRB event (eg., $E_{\mathrm{iso}} \sim 10^{54}$ ergs) can be easily produced by a supernova-like event (i.e., $E_{\mathrm{iso}} \sim 10^{50}$ ergs). We even do not need to make the embarrassing assumption that all the kinetic energy involved in the supernova-like event is beamed into a narrow cone to produce the GRB, which, as noted already, is not natural. Of course, in this case, the GRB rate in the Universe will be much higher correspondingly.

ACKNOWLEDGMENTS

REFERENCES

Akerlof C. et al., 1999, Nat, 398, 400

Berger E. et al., 2001, ApJ, submitted (astro-ph/0005465)

Biretta J. A., Sparks W. B., Macchetto F., 1999, ApJ, 520, 621

Blandford R. D., McKee C. F., 1976, Phys. Fluids, 19, 1130

Castro-Tirado A. et al., 1999, Sci, 283, 2069

Cheng K. S., Lu Y., 2000, MNRAS, in press (astro-ph/9906265)

Chevalier R. A., Li Z. Y., 2000, ApJ, 536, 195

Chiang J., Dermer C. D., 1999, ApJ, 512, 699

Costa E. et al., 1997, Nat, 387, 783

Dai Z. G., Huang Y. F., Lu T., 1999, ApJ, 520, 634

Dai Z. G., Lu T., 1998, MNRAS, 298, 87

Dai Z. G., Lu T., 1999, ApJ, 519, L155

Dar A., 1998, ApJ, 500, L93

Dar A., 1999, in Proceedings of "Neutrino Telescopes 1999" (ed. M. Baldo Ceolin), Venice (astro-ph/9905315)

Dermer C. D., Böttcher M., Chiang J., 1999a, ApJ, 515, L49

Dermer C. D., Chiang J., Böttcher M., 1999b, ApJ, 513, 656

Frail D. A. et al., 1997, Nat, 389, 261

Galama T. J. et al., 1997, Nat, 387, 479

Galama T. J. et al., 1998a, ApJ, 500, L101

Galama T. J., Wijers R. A. M. J., Bremer M., Groot P. J., Strom R. G., Kouveliotou C., van Paradijs J., 1998b, ApJ, 500, L97

Garcia M. R. et al., 1998, ApJ, 500, L105

Goodman J., 1986, ApJ, 308, L47

Groot P. J. et al., 1997, IAU Circ 6584

Harrison F. A. et al., 1999, ApJ, 523, L121

Huang Y. F., Dai Z. G., Wei D. M., Lu T., 1998a, MNRAS, 298, 459

Huang Y. F., Dai Z. G., Lu T., 1998b, A&A, 336, L69

Huang Y. F., Dai Z. G., Lu T., 1999a, Chin. Phys. Lett., 16, 775

Huang Y. F., Dai Z. G., Lu T., 1999b, MNRAS, 309, 513

Huang Y. F., Gou L. J., Dai Z. G., Lu T., 2000a, ApJ, 543, 90 (astro-ph/9910493)

Huang Y. F., Dai Z. G., Lu T., 2000b, MNRAS, 316, 943 (astro-ph/0005549)

Huang Y. F., Dai Z. G., Lu T., 2000c, Chin. Phys. Lett., 17, 778

Huang Y. F., Dai Z. G., Lu T., 2000d, A&A, 355, L43 (astro-ph/0002433)

Jensen B. L. et al., 2001, A&A, submitted (astro-ph/0005609)

Katz J., 1994, ApJ, 422, 248

Kulkarni S. R. et al., 1998, Nat, 393, 35

Kulkarni S. R. et al., 1999, Nat, 398, 389

Lamb D. Q., 2001, Phys. Report, in press (astro-ph/0005028)

Lee H. K., Brown G. E., Wijers R. A. M. J., 2000, ApJ, 536, 416

Masetti N. et al., 2000, A&A, 359, L23

Mészáros P., Laguna P., Rees M. J., 1993, ApJ, 415, 181

Mészáros P., Rees M. J., 1992, MNRAS, 257, 29P

Mészáros P., Rees M. J., 1997, ApJ, 476, 232

Mészáros P., Rees M. J., 1999, MNRAS, 306, L39

Mészáros P., Rees M. J., Papathanassiou H., 1994, ApJ, 432, 181

Mészáros P., Rees M. J., Wijers R. A. M. J., 1998, ApJ, 499, 301

Metzger M. et al., 1997, Nat, 387, 878

16

Moderski R., Sikora M., Bulik T., 2000, ApJ, 529, 151

Paczyński B., 1986, ApJ, 308, L43

Panaitescu A., Mészáros P., 1998, ApJ, 493, L31

Panaitescu A., Mészáros P., 1999, ApJ, 526, 707

Pedersen H. et al., 1998, ApJ, 496, 311

Perley R. A., Bridle A. H., Willis A. G., 1984, ApJS, 54, 291

Piran T., 1999, Phys. Report, 314, 575

Piro L. et al., 1998, A&A, 331, L41

Rees M. J., Mészáros P., 1992, MNRAS, 258, 41P

Rees M. J., Mészáros P., 1994, ApJ, 430, L93

Rhoads J., 1997, ApJ, 487, L1

Rhoads J., 1999, ApJ, 525, 737

Rhoads J., Fruchter A. S., 2001, ApJ, in press (astro-ph/0004057)

Sahu K. C. et al., 1997, Nat, 387, 476

Sari R., 1997, ApJ, 494, L49

Sari R., Narayan R., Piran T., 1996, ApJ, 473, 204

Sari R., Piran T., Halpern J. P., 1999, ApJ, 519, L17

Sari R., Piran T., Narayan R., 1998, ApJ, 497, L17

Shaviv N. J., Dar A., 1995, ApJ, 447, 863

Tavani M., 1997, ApJ, 483, L87

van Paradijs J. et al., 1997, Nat, 386, 686

van Paradijs J., Kouveliotou C., Wijers R. A. M. J., 2000, ARA&A, 38, 379

Vietri M., 1997, ApJ, 488, L105

Vreeswijk P. M. et al., 1999, ApJ, 523, 171

Wang X., Loeb A., 2001, ApJ, submitted (astro-ph/0009501)

Waxman E., 1997a, ApJ, 485, L5

Waxman E., 1997b, ApJ, 489, L33

Wijers R. A. M. J., 1998, Nat, 393, 13

Wijers R. A. M. J., Bloom J. S., Bagla J. S., Natarajan P., 1998, MNRAS, 294, 13

Wijers R. A. M. J., Galama T. J., 1999, ApJ, 523, 177

Wijers R. A. M. J., Rees M. J., Mészáros P., 1997, MNRAS, 288, L51

Wijers R. A. M. J. et al., 1999, ApJ, 523, 33

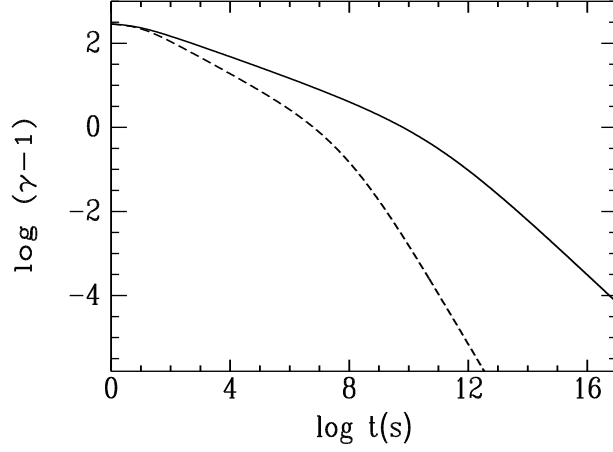**Figure 1.** Evolution of the Lorentz factor, γ, when $v_\perp \equiv 0$. The solid line corresponds to a cylindrical jet and the dashed line corresponds to a conical one. Parameters concerned here have been described in Section 4 of the main text.
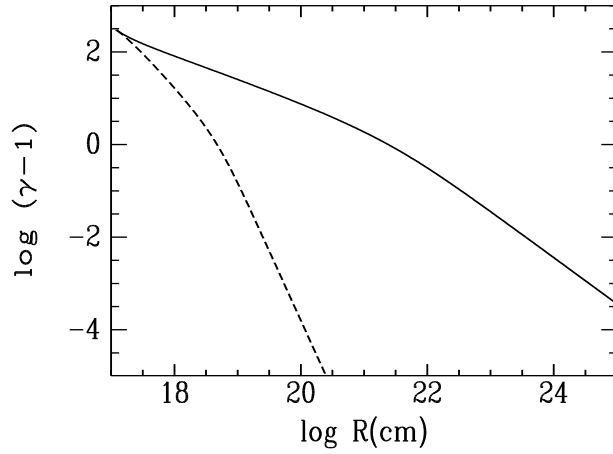

Figure 2. $\log(\gamma - 1)$ vs. $\log R$ for jets without lateral expansion ($v_\perp \equiv 0$). Line styles and parameters are the same as in Fig. 1.
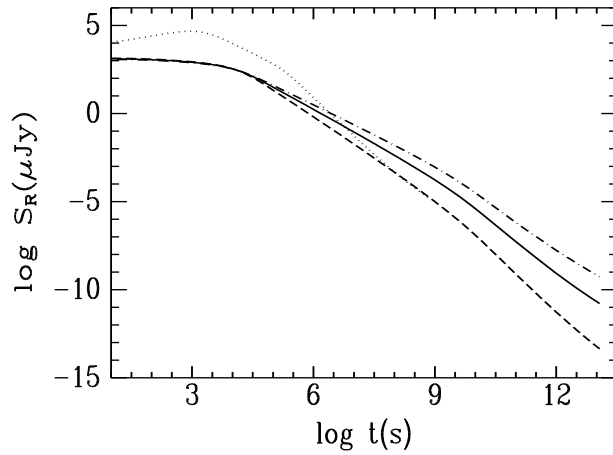

Figure 3. R band afterglows from beamed GRB ejecta without lateral expansion ($v_\perp \equiv 0$). The dotted line corresponds to a conical jet with $p = 2.5$. Other lines are for cylindrical jets which differ only in the parameter p: the dashed, solid and dash-dotted line corresponds to $p = 3$, 2.5 and 2.2 respectively. Other parameters have been given in Section 4 of the main text. The breaks at $t \sim 10^9$ s in the light curves for cylindrical jets are due to cooling of electrons.
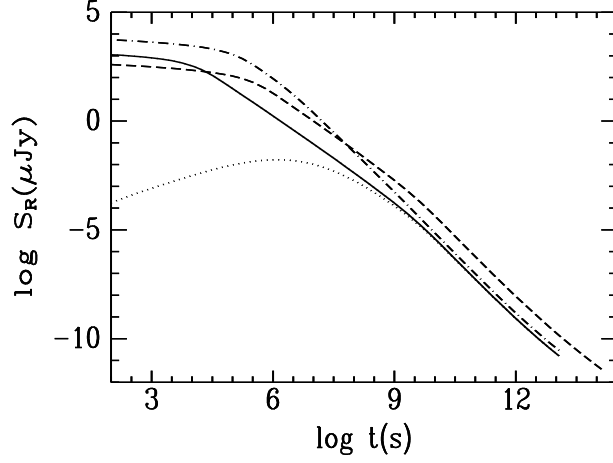
18

Figure 4. The effect of ξ_e, ξ_B^2 and Θ on the R band light curve ($v_\perp \equiv 0$ case). The solid line is plot with $\xi_e = 0.1$, $\xi_B^2 = 10^{-6}$, and $\Theta = 0$. Each of the other lines is plot with only one parameter altered with respect to the solid line. The dashed, dash-dotted and dotted lines correspond to $\xi_e = 0.5$, $\xi_B^2 = 10^{-4}$ and $\Theta = 0.1$ respectively. Other parameters not mentioned here have been described in Section 4 of the main text.
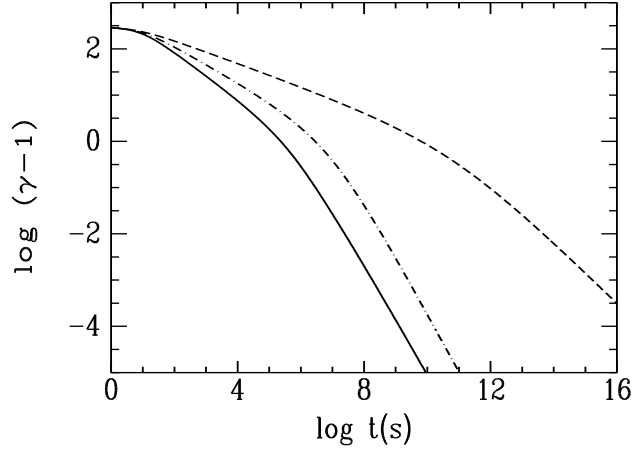

Figure 5. Evolution of the Lorentz factor, γ. The solid line corresponds to a cylindrical jet with $v_\perp \equiv c_s$. For comparison, the dash-dotted line corresponds to a conical jet with $v_\perp \equiv c_s$, and the dashed line is for a cylindrical jet without lateral expansion. Parameters are the same as in Fig. 1.
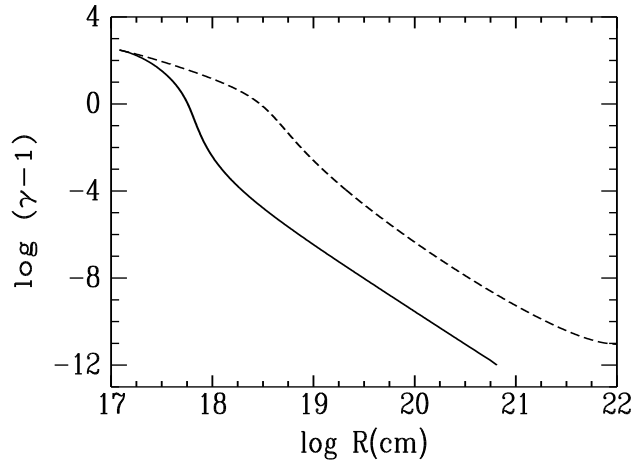

Figure 6. $\log(\gamma - 1)$ vs. $\log R$ for jets with lateral expansion $v_\perp \equiv c_s$. The solid line corresponds to a cylindrical jet and the dashed line corresponds to a conical one. Parameters are the same as in Fig. 1.
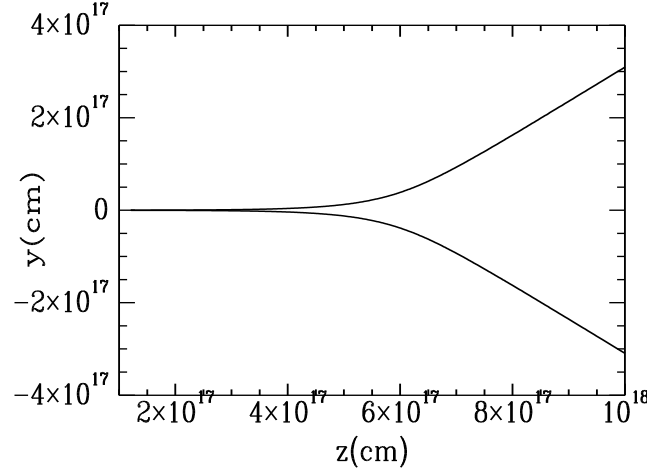
Figure 7. Schematic illustration of the lateral expansion of a cylindrical jet on the $y - z$ plane. z-axis is the symmetry axis of the jet and the lateral expansion is along y-axis. Parameters are the same as those associated with the solid line in Fig. 6.
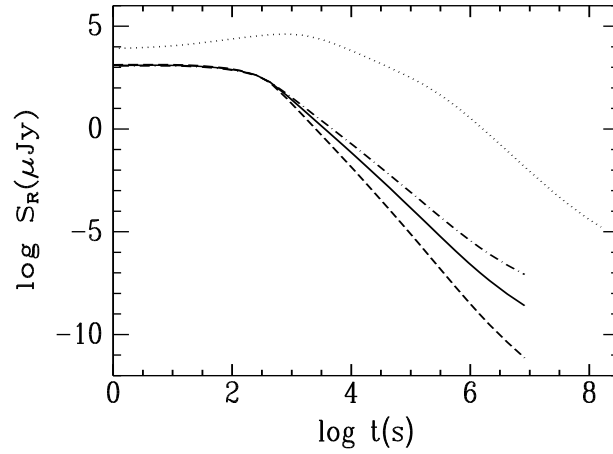

Figure 8. R band afterglows from beamed GRB ejecta with lateral expansion ($v_\perp \equiv c_s$). The dotted line corresponds to a conical jet with $p = 2.5$, other lines are for cylindrical jets which differ only in the parameter p. The dash-dotted, solid and the dashed line corresponds to $p = 2.2, 2.5$ and 3.0 respectively. Other parameters not mentioned here have been described in Section 4 of the main text. Note that the cylindrical jets here are already non-relativistic when $t > 10^6$ s.
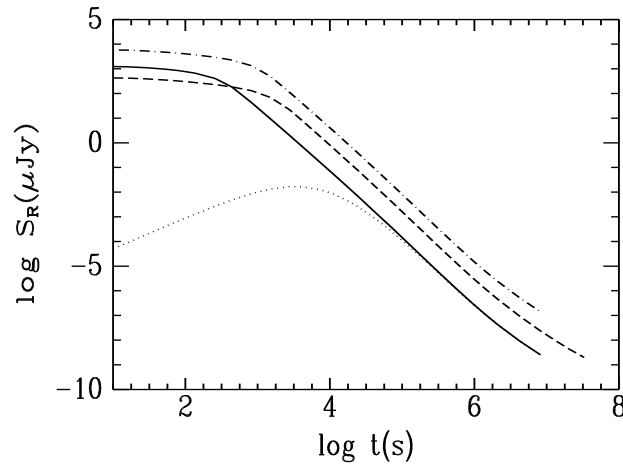

Figure 9. The effect of ξ_e, ξ_B^2 and Θ on the R band light curve ($v_\perp \equiv c_s$ case). The solid line is plot with $\xi_e = 0.1$, $\xi_B^2 = 10^{-6}$ and $\Theta = 0$. Each of the other lines is plot with only one parameter altered with respect to the solid line. The dashed, dash-dotted and dotted lines correspond to $\xi_e = 0.5$, $\xi_B^2 = 10^{-4}$ and $\Theta = 0.1$ respectively. Other parameters not mentioned here have been described in Section 4 of the main text.